Offline commissioning and performance of a multi-reflection time-of-flight mass analyzer with a new configuration

Wen-Xue Huang[a,c,d], Yong-Sheng Wang[a,b,c,d], Yu-Lin Tian[a,c,d,*], Jun-Ying Wang[a,c], Yue Wang[a,c], Zai-Guo Gan[a,c,d], Hu-Shan Xu[a,c,d]

[a] *CAS Key Laboratory of High Precision Nuclear Spectroscopy, Institute of Modern Physics, Chinese Academy of Sciences, Lanzhou, 730000, China*
[b] *School of Nuclear Science and Technology, Lanzhou University, Lanzhou, 730000, China*
[c] *Advanced Energy Science and Technology Guangdong Laboratory, Huizhou, 516000, Guangdong Prov., China*
[d] *School of Nuclear Science and Technology, University of Chinese Academy of Sciences, Beijing, 100049, China*

Abstract

To precisely measure atomic masses and select isotopes of interest, a multi-reflection time-of-flight mass spectrometer is being built at SHANS (Spectrometer for Heavy Atom and Nuclear Structure). Its mass analyzer with a new configuration different from the existed ones has been commissioned successfully with a chopped ^{133}Cs beam by using a Bradbury-Nielsen gate. The potentials on all electrodes have been optimized by using two-dimensional potential scan method. With the optimized parameter set, an efficiency of 50% has been obtained. The mass resolving power with a time-of-flight of 12.9 ms has been measured to be 74,000, and it has reached 90,000 with a longer time-of-flight of ∼20 ms.

*Corresponding authors.
Email addresses: huangwx@impcas.ac.cn (Wen-Xue Huang), yltianok@impcas.ac.cn (Yu-Lin Tian)

Keywords:
Multi-reflection time-of-flight mass spectrometer, Mass resolving power, Mass measurement, Isobaric separation

1. Introduction

In recent years, more than a dozen of multi-reflection time-of-flight mass spectrometers (MRTOF-MS) have been or will be constructed all over the world [1–11]. The tasks of these devices are to perform accurate mass measurements and isobaric separation, and fruitful experimental results have been achieved already [12–19]. Plaß et al. [20] reviewed the MRTOF-MS developments for the research with short-lived nuclei and different instrumental implementations. At the Institute of Modern Physics, Chinese Academy of Sciences (IMP/CAS), we are developing an MRTOF-MS to attach to the end of SHANS (Spectrometer for Heavy Atom and Nuclear Structure [21]) to precisely measure atomic masses and select isotopes of interest.

The conceptual design of the low energy mass spectrometer at SHANS was described in Ref. [22]. It consists of a degrader, cryogenic gas catcher, quadrupole ion beam guide, radiofrequency quadrupole cooler and buncher, MRTOF mass analyzer and time-of-flight detector. The MRTOF mass analyzer plays an important role as the ions fly in it and are separated in time according to their mass-to-charge ratios. The electrode design and the potential applied must be chosen carefully such that the analyzer is time focusing, i.e. that time-of-flight differences because of initial energies, positions and angles of the injected ions are reduced as small as possible.

Since the number of electrodes affects the potential smoothness along the

optical axis and determines the number of power supplies, we designed a new type of MRTOF mass analyzer with a different configuration, in which each mirror consists of five electrodes rather than four [23] or eight [3, 24, 25]. The design and computer simulation have been reported in previous papers [8, 26].

In this paper, we will concentrate on the offline commissioning of the MRTOF mass analyzer and report the achieved performances in detail.

2. Experimental setup

Fig. 1 shows schematically the experimental beam line used for the offline commissioning. A continuous $^{133}Cs^{1+}$ beam is produced by a heated alkali ion source emitter (a) from HeatWave Labs [27] followed by a skimmer (b) and an extraction electrode (c). The emitter is connected to a supporting electrode floating at a potential of ∼190 V above the ground, thereby defining the initial kinetic energy of the ions. The potentials on the skimmer and the extraction electrode are 155 V and 100 V, respectively. Then a Bradbury-Nielsen gate (BNG, e) [28], which is made of stainless steel wires with a diameter of 50 μm and a spacing between wires of 250 μm, is employed to bunch the beam by switching on/off the ±28 V potentials applied on two sets of the parallel wires, named as BNG1 and BNG2.

In order to reduce the emittance by limiting the radial spread of the beam and thus improve its quality, three apertures are used in combination. The first one is in the skimmer with a diameter of 3 mm, the second one is in the flange (d) before the BNG with a diameter of 6 mm and the third one (f) is behind the BNG with a diameter of 2 mm. Afterwards, an einzel lens (g)

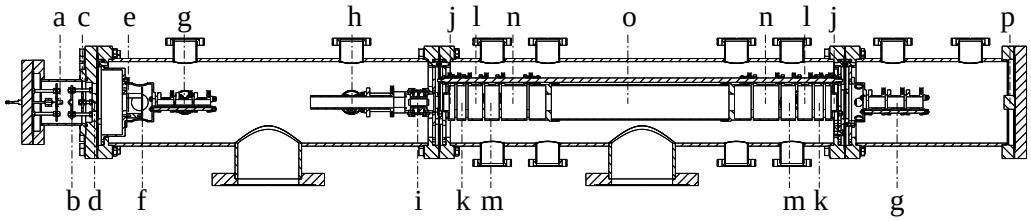

Figure 1: Schematic drawing of the offline commissioning beam line: a – ion source emitter, b – skimmer, c – extraction electrode, d & f – collimator, e – BNG, g – einzel lens, h – Acc-PDT, i – deflector, j – mirror electrode M1, k – M2, l – M3, m – M4, n – lens electrode L, o – drift tube DT, p – detector.

with potentials of 0, 35 V, 0 is used to focus the pulsed beam to the middle of the acceleration pulsed drift tube (Acc-PDT, h), where the ion bunches are accelerated to a kinetic energy of 1500 eV by switching its potential from 0 to ∼1310 V to match the requirement of the MRTOF mass analyzer. A cylindrical deflector (i) cut equally into 4 parts is placed between the Acc-PDT and the mass analyzer to adjust the ion beam in the radial direction, and the potentials applied on these electrodes are 0, 28 V, 38 V and 0, respectively.

The MRTOF mass analyzer consists of four pairs of mirror electrodes M1–M4 (j, k, l, m), a pair of lens electrodes L (n) and a drift tube DT (o). The details of the MRTOF structure design can be found in [8, 26]. The mirror electrodes, from the outermost ends to the middle, have lengths of 20, 16, 26, and 26 mm, respectively, the lens electrode has a length of 46 mm, and the intermediate drift tube has a length of 400 mm. The adjacent electrodes are insulated by 4 mm thick ceramic spacers, and the total length of this analyzer is 708 mm. The diameter of the electrodes is 60 mm, four

reduced apertures with diameter of 30 mm located on the outer ends of M1 and DT are added for electric shielding.

The ions are captured by using the in-trap potential lift method [29], in which the kinetic energy of the ions are reduced below the barrier of mirror electrodes by switching off the potential on the drift tube. After flying a certain number of laps, the bunches are released by switching on the potential on the drift tube and hit a MagneTOF detector from ETP Ion Detect^{TM} [30] placed at the end of the beam line. The time of flight (TOF) from the BNG to this detector is recorded by a SR430 multichannel scaler (MCS) from Stanford Research Systems [31].

Two sets of vacuum pump from Edward Vacuum [32] are used to achieve an environment with a residual gas pressure better than 3×10^{-8} mbar. High voltage (HV) modules with high precision and stability from ISEG Spezialelektronik GmbH [33] are used to drive the electrodes. Fast solid switches from BEHLKE Power Electronics [34] and CGC Instruments [35] are employed to switch on/off the voltages varying with time.

The whole system is controlled remotely by a specialized distributed real-time control system based on EPICS [36]. Fig. 2(a) shows the fast control diagram. A PCI-7813R field programmable gate array (FPGA) module from National Instrument [37] followed by a TTL line driver is used to trigger the BNG, Acc-PDT, DT switches and the SR430 MCS. The measurement cycle is depicted in Fig. 2(b). It consists of five channels synchronized with a precision of 25 ns. A cycle starts when the BNG is opened. The opening time was optimized to be 0.15 μs. Twenty three μs later, the potential on the Acc-PDT is switched on when the bunched ions reach the middle of the

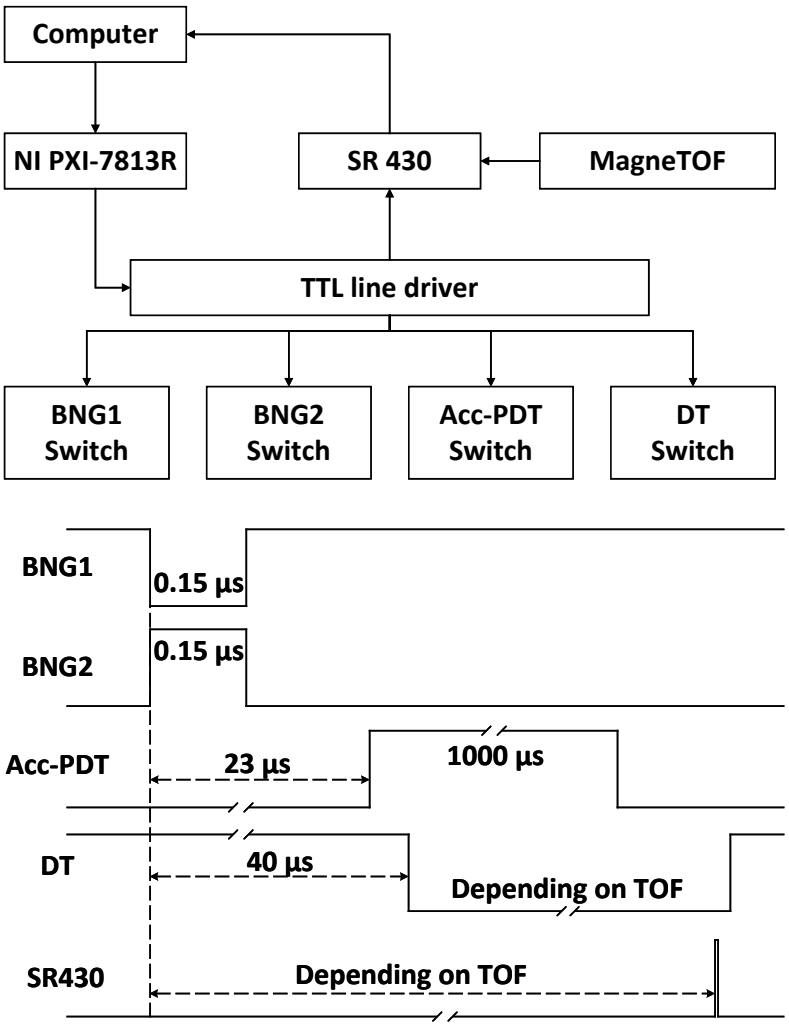

Figure 2: Top: Fast control diagram used for the offline commissioning. Bottom: Overview of a measurement cycle (not in scale).

Acc-PDT and it lasts 1 ms, which is long enough to ensure that all the ions leave the Acc-PDT and be accelerated. The ions are captured 40 μs after being bunched when they reach the middle of DT and released after flying a certain number of laps, which determines the duration. As the total TOF of the ions is much longer than the maximum that the SR430 MCS can be recorded, the trigger for the MCS has to be delayed to let the whole TOF spectrum be recorded. This delay time is varied according to the number of laps which the ions fly in the analyzer, as well as the bin width and the bins per record of the MCS. Typically the bin width of 40 ns or 5 ns (the narrowest available) are used during the offline commissioning.

3. Optimization of the MRTOF mass analyzer

The goal of the optimization process is to find the electrode potentials that maximize the resolving power with a good symmetry of the TOF peak. The mass resolving power is defined as

$$MRP = TOF/2/\Delta TOF,$$

where TOF is the total time-of-flight and ΔTOF is the full width at half maximum (FWHM) of the peak.

Due to the impact of image aberration, field imperfection and mechanical misalignment, the peaks of TOF spectrum are asymmetrical [38]. In order to quantify the symmetry of the TOF peak and then easily pick out the potential parameters with good symmetry during the optimization, the coefficient of determination (COD) of Gaussian fit has been calculated. The COD is

expressed as

$$R^2 = 1 - \sum_{i=1}^{n}(y_{\mathrm{i}} - \mathrm{f(x_i)})^2 / \sum_{\mathrm{i=1}}^{\mathrm{n}} \mathrm{y_i^2},$$

where y_{i} is the experimental data and $f(x_{\mathrm{i}})$ is the fitted value with the statistical model. The minimum possible value of R^2 is 0 and the maximum is 1. The COD measures how well a statistical model predicts an outcome. Since Gaussian distribution is one of the main components of the TOF peak and distinctly symmetrical, we can employ the COD of Gaussian fitting to describe its symmetry. The closer the COD of Gaussian fitting is to 1, the closer the TOF peak has the Gaussian distribution, and the more symmetrical the peak is. One cannot determine the range of COD of Gaussian fitting for a reasonable symmetry, but after analyzing the spectrum, we found that long tails appears in the spectrum when R^2 is less than 0.980. Note that the Gaussian fitting is used if not specified in this paper.

A Python code was developed to set the timing and potential parameters and analyze the experimental results online. The TOF, ΔTOF and R^2 values were quickly calculated in real time after a measurement finished and were stored for future analysis along with the potential parameters.

The switching times for accelerating ions by the Acc-PDT, capturing and releasing ions by the DT were scanned to let these operations start when the ions are near the middle of the Acc–PDT and DT. One-dimensional potential scans on the skimmer, extraction electrode, BNG and einzel lens and two-dimensional on the deflector were performed for narrow beam width and high transport efficiency. The optimized values have been described in Section 2.

For the optimization of MRTOF mass analyzer, potentials on the adjacent electrodes were scanned in a two-dimensional way over a given range and a

linear progression through electrodes as M1 vs. M2, M2 vs. M3, M3 vs. M4, M4 vs. L and L vs. DT was followed during the whole optimization process. It would be very time-consuming to find the best point(s) in a large space with a small step size, so a global search and a local refinement were employed. During the global search, the potential ranges were as large as tens of volts and the step size was 0.5 V or larger. Some sub-regions with relatively narrow distribution and good symmetry were found after the global search. These sub-regions were selected for local refinement with a step size of 0.02 V or smaller.

The simulated potentials by using SIMION [39] were chosen as the starting points of the optimization. All electrodes of the MRTOF mass analyzer have been optimized based on 300 laps. In order to have sufficient statistics to fit the TOF spectrum, 10,000 bunches were recorded in each measurement.

As an example, Fig. 3(a)-(c) show two-dimensional TOF, MRP and R^2 contour plots when varying the potentials applied on the M1 and M2. Fig. 3(d) shows the MRP contour plots with $R^2 > 0.980$. In this case, the maximum MRP with a good R^2 located at M1 = 1073.5 V and M2 = 886.0 V is the optimal choice. We adopted 1073.5 V as our optimal potential for M1 and continued two-dimensional scan on the potentials on M2 and M3. This process repeated as needed until all the potentials on the electrodes had been optimized.

4. Results and discussion

Table 1 lists the optimal potentials applied on the mirrors electrodes, lens electrode and drift tube after the whole optimization process. With this

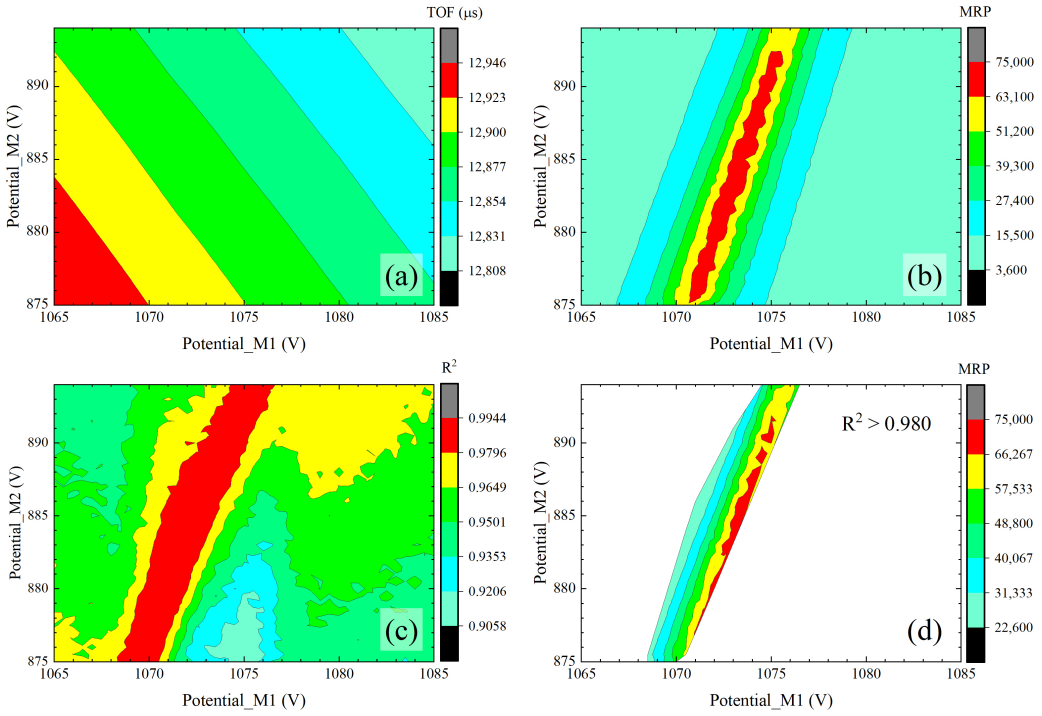

Figure 3: (a)-(c): Two-dimensional contour plots of TOF, MRP and R^2 as a function of the M1 and M2 electrode potentials; (d) Same as (b) but with $R^2 > 0.980$.

Table 1: Optimized potentials and fitted slopes of the time-of-flight deviation with applied potential on mirrors electrodes (M1–M4), lens electrode (L) and drift tube (DT). ppm stands for parts-in-million.

Electrode	M1	M2	M3	M4	L	DT
Potential (V)	1073.30	884.85	472.67	608.67	−1852.80	672.30
Slope (ns/ppm)	-4.630(7)	-2.254(2)	0.670(2)	0.655(2)	-0.897(2)	-0.062(3)

parameter set, we can investigate the TOF spectra at different number of laps and study the influence of power supply stability.

4.1. Performances at different laps

Fig. 4 shows the measured TOF, ΔTOF, MRP and R^2 at different laps which the ions fly in the mass analyzer. As the figures indicate, all these values are functions of number of laps. The TOF from the BNG to the detector increases linearly with the number of laps with a slope of 42.758(1) μs per lap and the ions can be stored in the analyzer up to 65 ms or even longer.

The MRP increases as increasing number of laps until ∼400 and reaches a plateau around 90,000. Fig. 5 shows the TOF spectra obtained at 300 laps where the optimization process has been taken and 500 laps where the maximum MRP obtained. The MRP reaches 74,000 at 300 laps corresponding a TOF of 12.9 ms, and it reaches 90,000 at 500 laps corresponding a TOF of 21.4 ms. Shown in Fig. 4(d), the R^2 is greater than 0.980 in most cases, but it becomes smaller and thus the symmetry of the peak becomes worse when the number of laps is far from 300, where the optimization was performed.

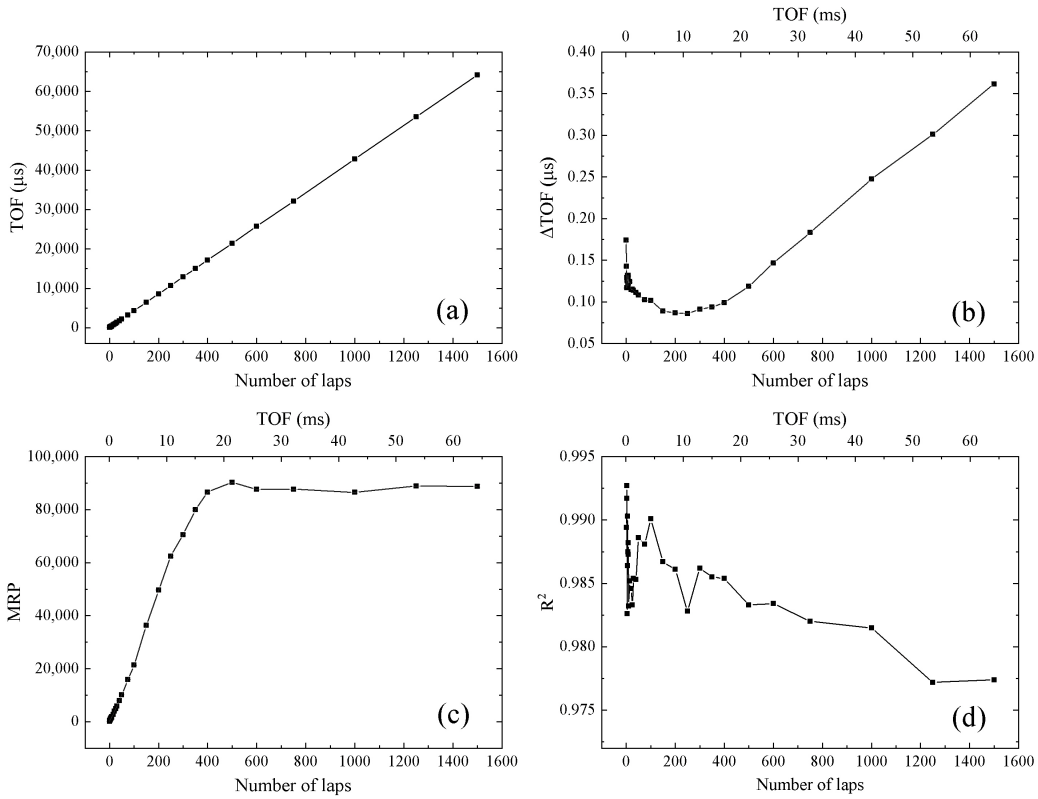

Figure 4: The measured TOF (a), ΔTOF (b), MRP (c) and R^2 (d) as a function of number of laps with the optimized parameter set in Table 1.

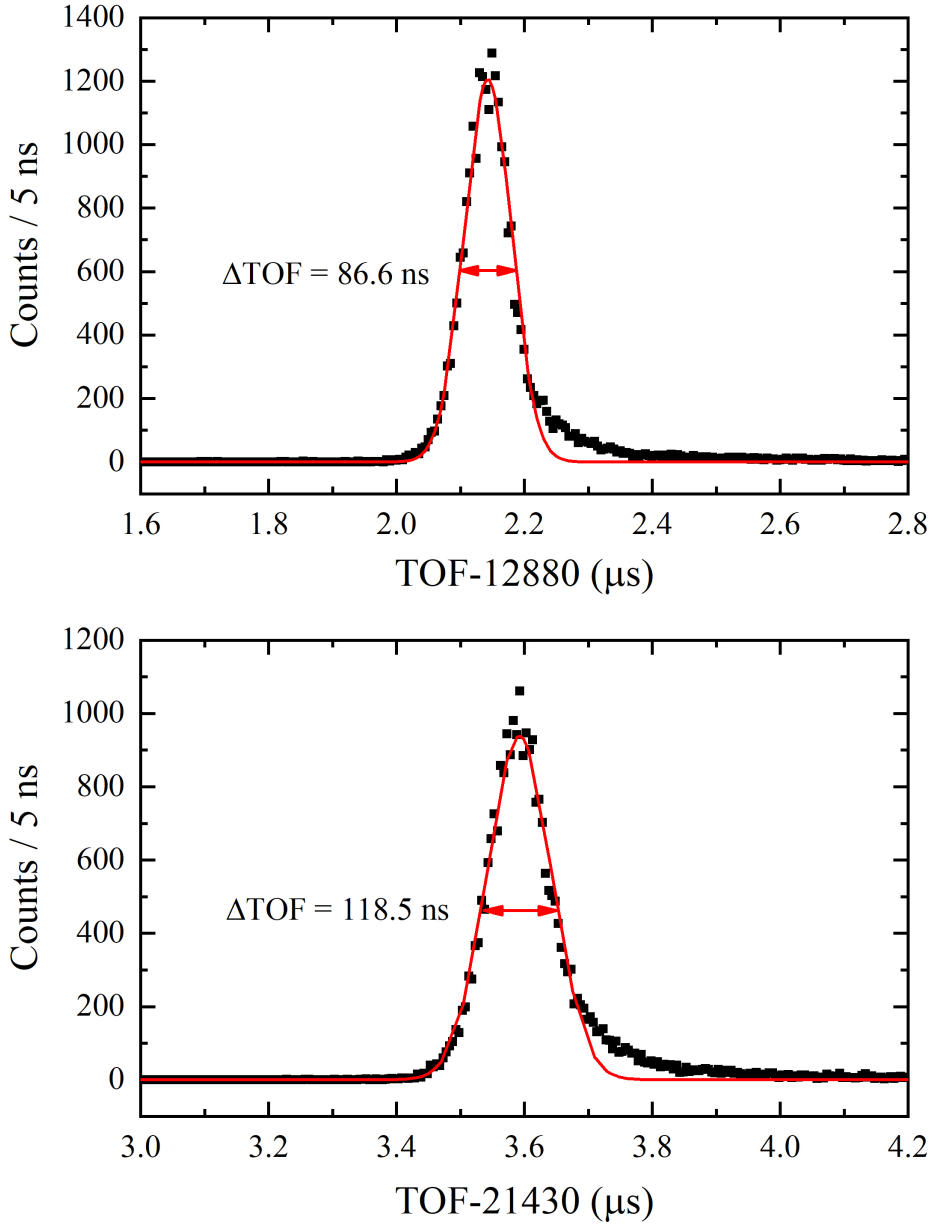

Figure 5: The TOF spectra obtained at 300 laps where the optimization process was taken (top) and at 500 laps where the maximum MRP obtained (bottom). The red curves are the fitted results with a Gaussian function.

The transport efficiency is defined as the ratio of the total number of counts after a certain number of laps in the analyzer to the total number of counts obtained when shooting through the analyzer. Fig. 6 shows the measured efficiency at different laps. The efficiency decreases as increasing the number of laps. It clearly shows that about 40% of the ions are lost in the first 10 laps and the remaining ions tend to stay in the analyzer for the remaining number of laps. The efficiency keeps at ∼50% in the 100-500 laps and decreases slight afterwards. At 1500 laps, we still have an efficiency more than 40%. The losses can be explained as two components, the quick one could be due to the acceptance of the analyzer, the emittance of the beam or a mechanical misalignment and the slow one due to the collision with residual gas inside the analyzer. The relatively higher efficiency compared to the values in Ref. [10] should be due to the larger inner diameter and thus a larger acceptance of our analyzer.

4.2. Effect of potential inaccuracy

Fig. 7 shows how the TOF, ΔTOF and MRP change when varying the potentials on each pair of electrodes. The potential deviation is defined as $(V - V_{opt})/V_{opt}$, where V is the potential applied on electrode and V_{opt} is the optimized potential listed in Table 1. For all the electrodes of the analyzer, the TOF changes linearly with the change of potentials and the sensitivity was determined quantitatively by the slopes of linear fit listed in Table 1. It shows that TOF is most sensitive to the potentials on M1 and M2, and a voltage deviation of 0.1 V on M1 and M2 can result in 0.46 μs and 0.25 μs TOF change, respectively. For MRP, the potentials on M1 and DT are the most sensitive ones. It clearly shows that the potential on M1 is most critical

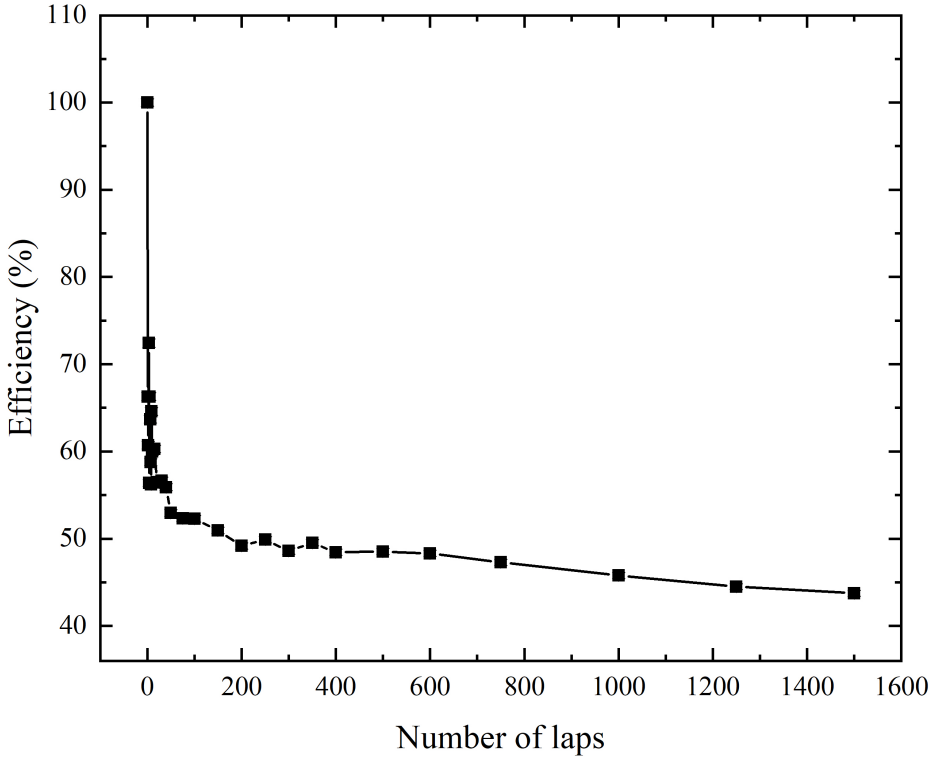

Figure 6: The measured transport efficiency as a function of number of laps with the optimized parameter set in Table 1.

to the performance of the mass analyzer. It is understandable that the ions turn around at the place of M1 and a small deviation from the ideal potential may result in a significant change of the ion trajectory. The change of MRP from the DT potential can be explained by the change of the energy of the ions trapped inside the analyzer. The MRP is not sensitive to the potentials on other electrodes except M1 and DT.

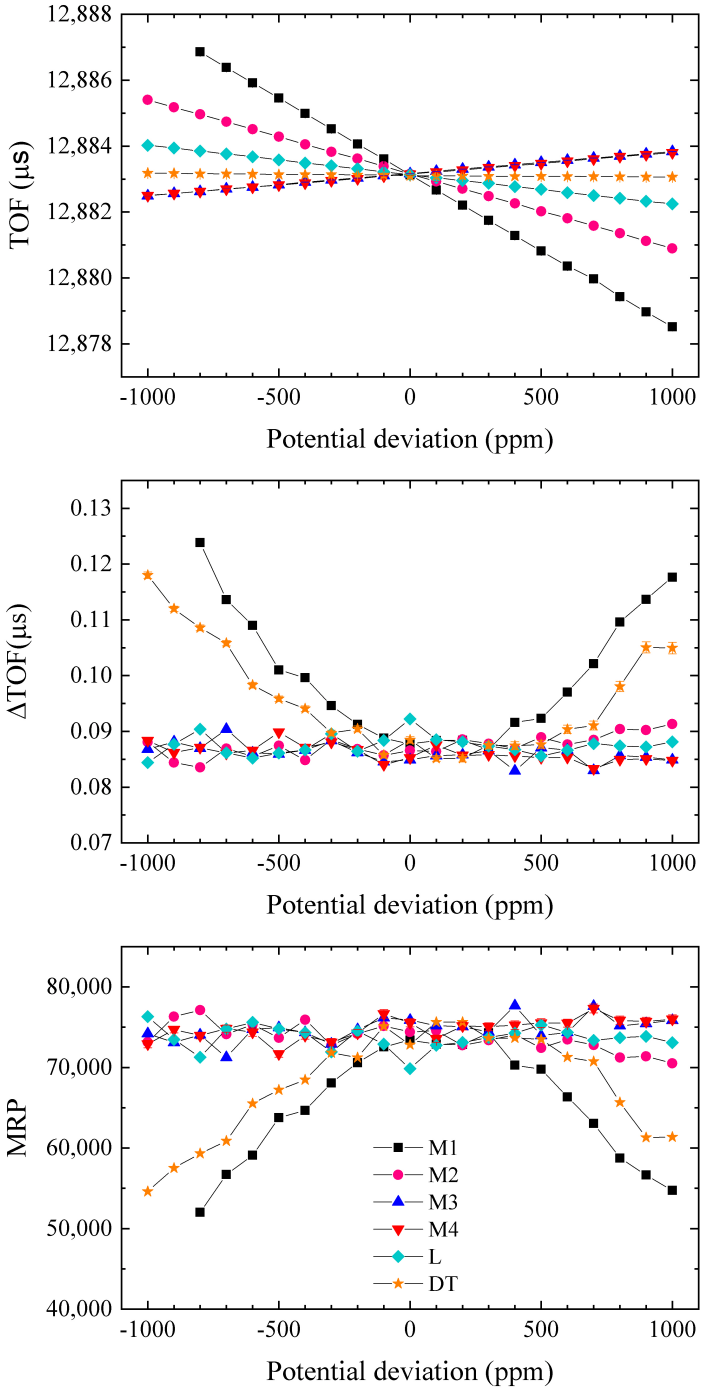

Figure 7: The change of TOF (top), ΔTOF (middle) and MRP (bottom) as a function of deviation of potentials applied on the electrodes. ppm stands for parts-in-million. Note that the points of M3 and M4 are almost overlapped and need to be carefully distinguished.

4.3. Long time stability test

In order to observe the behavior of the TOF spectrum as a function of elapsed time, we took a long time measurement with the optimized potentials listed in Table 1 at 300 laps. Fig. 8 shows the measured TOF and MRP obtained in a continuous 52-hour measurement. It clearly shows that the TOF drifts with the elapsed time with a period of ∼24 hours, which should be explained by the drift of the electrical power during the day and night, and also maybe the change of the environmental temperature. The maximal changes of TOF reached 0.2 μs. The MRP also fluctuates, but does not have a regular period.

The symmetry of the TOF distribution can be studied by the 1167 spectra obtained during this 52-hour measurement. Fig. 9 shows the sum peak after re-centering the TOF peaks to correct for temporal drifts and then adding them together. As it shows, the peak is symmetric, except for a small long tail on the right side. That could be the result of having a non-ideal trapping potential in the analyzer and an asymmetric distribution of the beam at the entrance of the analyzer. The sum peak can be fitted very well by using a Hyper-EMG function [38] and the ΔTOF and R^2 were derived to be 67.9(1) ns and 0.999, respectively. The corresponding values by using a Gaussian fit are 88.9(1) ns and 0.989.

5. Summary

A multi-reflection time-of-flight mass analyzer with a new configuration has been constructed and successfully commissioned. The potentials on all electrodes have been optimized by using two-dimensional potential scan

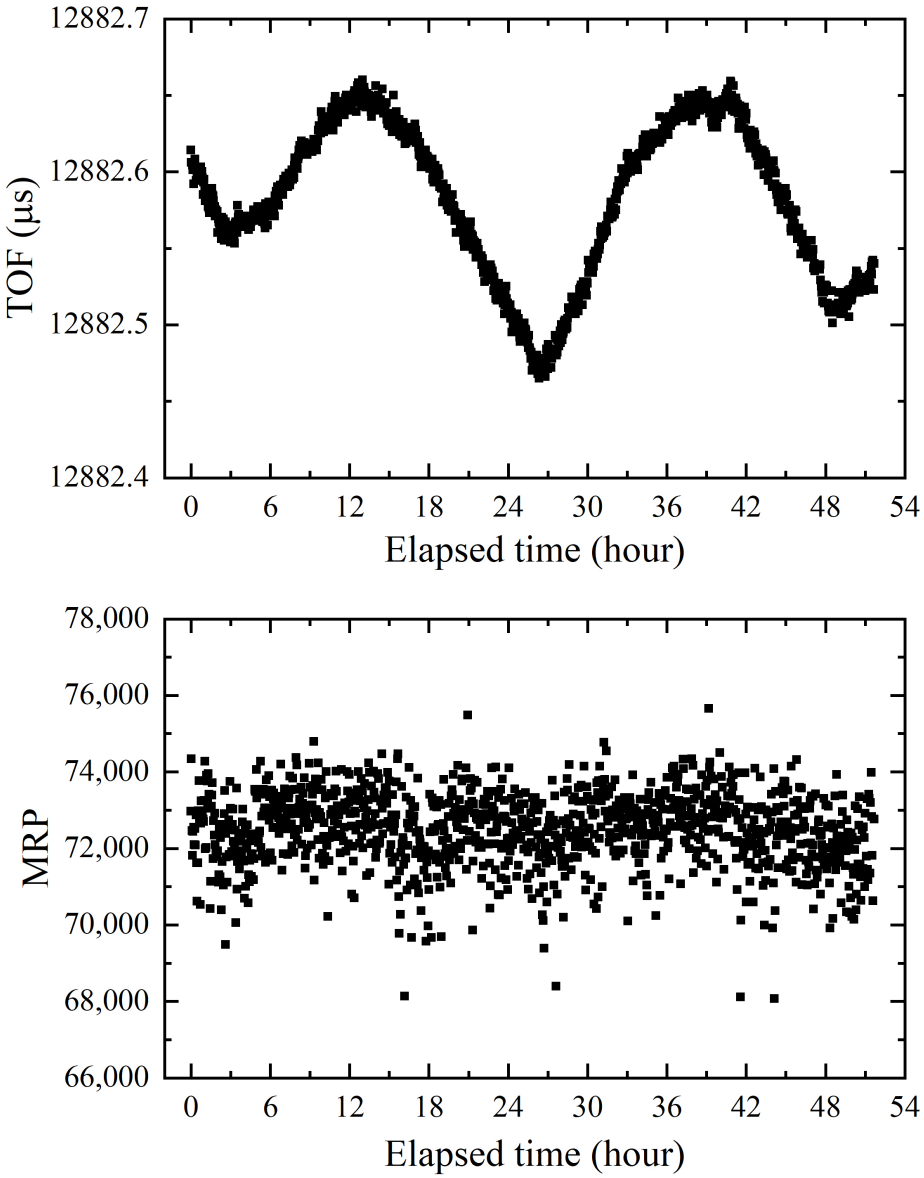

Figure 8: The measured TOF (top) and MRP (bottom) as a function of elapsed time of the measurement with the optimized parameter set at 300 laps.

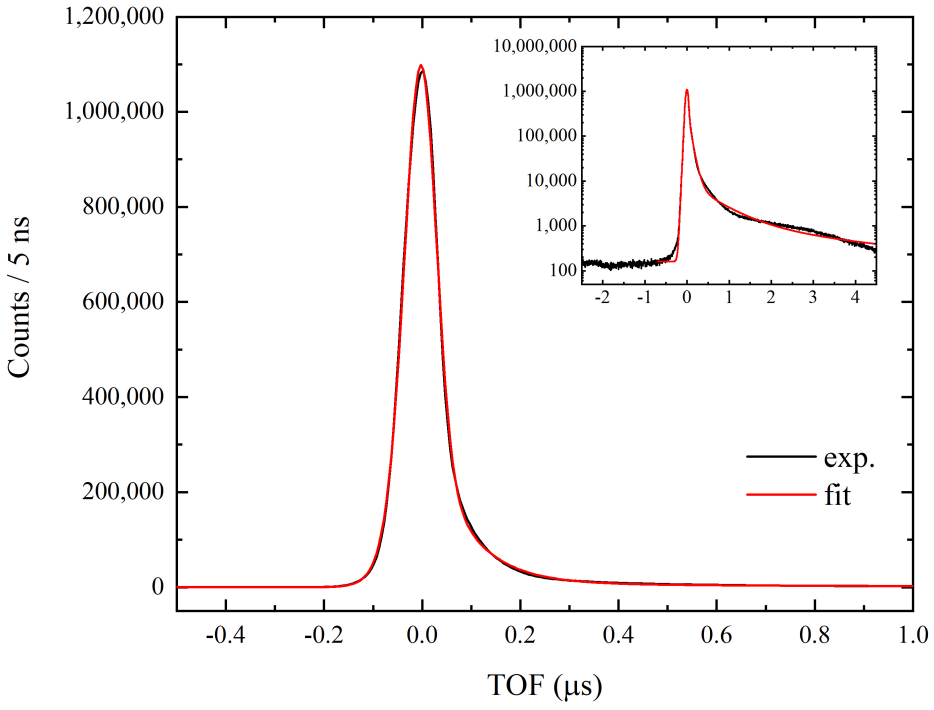

Figure 9: The sum peak of 1167 re-centered peaks obtained in a continuous 52-hour measurement at 300 laps in linear scale and in log scale (top right corner). The TOF peak is fitted by using a Hyper-EMG function.

method.

The coefficient of determination of Gaussian fitting has been calculated and used as a probe to quickly and accurately pick out the potential parameters with good symmetry. With the optimized potentials applied on the electrodes, the ions can be stored in the analyzer up to 65 ms or even longer. An efficiency of 50% has been obtained. The mass resolving power at 300 laps with a time-of-flight of 12.9 ms has been measured to be 74,000, and it can reach 90,000 with a longer time-of-flight of ∼20 ms. The mass resolving power is limited by the rather broad beam chopped by the Bradbury-Nielsen gate and will be improved by using high quality pulsed beam with narrow bunch width and small emittance. It will be installed at SHANS to directly measure the masses and separate the isobars of fusion evaporation reaction products.

CRediT authorship contribution statement

W.X. Huang: Supervision, Conceptualization, Investigation, Methodology, Software, Formal analysis, Visualization, Writing - original draft & review & editing, Funding acquisition. **Y.S. Wang:** Investigation, Methodology, Writing - review & editing. **Y.L. Tian:** Investigation, Conceptualization, Methodology, Formal analysis, Visualization, Writing - original draft, Funding acquisition. **J.Y. Wang:** Investigation, Methodology, Writing - review & editing. **Y. Wang:** Investigation. **Z.G. Gan:** Supervision, Conceptualization, Investigation, Funding acquisition. **H.S. Xu:** Supervision, Funding acquisition.

Declaration of competing interest

The authors declare that they have no known competing financial interests or personal relationships that could have appeared to influence the work reported in this paper.

Acknowledgments

This work was supported by the Frontier Science Key Project of the Chinese Academy of Sciences (Grant No. ZDBS-LY-SLH017), the Guangdong Major Project of Basic and Applied Basic Research (Grant No. 2021B0301030006), the National Natural Science Foundation of China (Grants No. 12075286, 11675224, 11405243), the CAS Light of West China Program (2022-04), the National Key R&D Program of China (Contract No. 2018YFA0404402) and the Strategic Priority Research Program of Chinese Academy of Sciences (Grant No. XDB34010000).

References

[1] R. N. Wolf, D. Beck, K. Blaum, C. Bohm, C. Borgmann, M. Breitenfeldt, F. Herfurth, A. Herlert, M. Kowalska, S. Kreim, D. Lunney, S. Naimi, D. Neidherr, M. Rosenbusch, L. Schweikhard, J. Stanja, F. Wienholtz, K. Zuber, On-line separation of short-lived nuclei by a multi-reflection time-of-flight device, Nucl. Instrum. Methods A 686 (2012) 82–90. doi:10.1016/j.nima.2012.05.067.

[2] T. Dickel, W. R. Plaß, A. Becker, U. Czok, H. Geissel, E. Haettner, C. Jesch, W. Kinsel, M. Petrick, C. Scheidenberger, A. Simon, M. I.

Yavor, A high-performance multiple-reflection time-of-flight mass spectrometer and isobar separator for the research with exotic nuclei, Nucl. Instrum. Methods A 777 (2015) 172–188. doi:10.1016/j.nima.2014.12.094.

[3] P. Schury, M. Wada, Y. Ito, F. Arai, S. Naimi, T. Sonoda, H. Wollnik, V. A. Shchepunov, C. Smorra, C. Yuan, A high-resolution multi-reflection time-of-flight mass spectrograph for precision mass measurements at RIKEN/SLOWRI, Nucl. Instrum. Methods B 335 (2014) 39–53. doi:10.1016/j.nimb.2014.05.016.

[4] P. Schury, M. Wada, Y. Ito, D. Kaji, F. Arai, M. MacCormick, I. Murray, H. Haba, S. Jeong, S. Kimura, H. Koura, H. Miyatake, K. Morimoto, K. Morita, A. Ozawa, M. Rosenbusch, M. Reponen, P. A. Söderström, A. Takamine, T. Tanaka, H. Wollnik, First online multireflection time-of-flight mass measurements of isobar chains produced by fusion-evaporation reactions: Toward identification of superheavy elements via mass spectroscopy, Phys. Rev. C 95 (2017) 011305. doi:10.1103/PhysRevC.95.011305.

[5] T. Y. Hirsh, N. Paul, M. Burkey, A. Aprahamian, F. Buchinger, S. Caldwell, J. A. Clark, A. F. Levand, L. L. Ying, S. T. Marley, G. E. Morgan, A. Nystrom, R. Orford, A. P. Galván, J. Rohrer, G. Savard, K. S. Sharma, K. Siegl, First operation and mass separation with the CARIBU MR-TOF, Nucl. Instrum. Methods B 376 (2016) 229–232. doi:10.1016/j.nimb.2015.12.037.

[6] V. S. Kolhinen, T. Eronen, D. Gorelov, J. Hakala, A. Joki-

nen, K. Jokiranta, A. Kankainen, M. Koikkalainen, J. Koponen, H. Kulmala, M. Lantz, A. Mattera, I. D. Moore, H. Penttilä, T. Pikkarainen, I. Pohjlainen, M. Reponen, S. Rinta-Antila, J. Rissanen, C. Rodríguez Triguero, K. Rytkönen, A. Saastamoinen, A. Solders, V. Sonnenschein, J. Äystö, Recommissioning of JYFLTRAP at the new IGISOL-4 facility, Nucl. Instrum. Methods B 317 (2013) 506–509. doi:10.1016/j.nimb.2013.07.050.

[7] P. Chauveau, P. Delahaye, G. De France, S. El Abir, J. Lory, Y. Merrer, M. Rosenbusch, L. Schweikhard, R. N. Wolf, PILGRIM, a multi-reflection time-of-flight mass spectrometer for SPIRAL2-S^3 at GANIL, Nucl. Instrum. Methods B 376 (2016) 211–215. doi:10.1016/j.nimb.2016.01.025.

[8] Y. L. Tian, Y. S. Wang, J. Y. Wang, X. H. Zhou, W. X. Huang, Designing a multi-reflection time-of-flight mass analyzer for LPT, Int. J. Mass Spectrom. 408 (2016) 28–32. doi:10.1016/j.ijms.2016.08.013.

[9] J. W. Yoon, Y.-H. Park, K.-B. Im, G. D. Kim, Y. K. Kim, Design study for a multi-reflection time-of-flight mass spectrograph for very short lived nuclei. doi:10.7566/JPSCP.6.030120.

[10] B. Liu, M. Brodeur, D. P. Burdette, J. M. Kelly, T. Kim, J. Long, P. D. O'Malley, The performance of the commissioned Notre Dame multi-reflection time-of-flight mass spectrometer, Nucl. Instrum. Methods A 985 (2021) 164679. doi:10.1016/j.nima.2020.164679.

[11] M. Reiter, S. A. S. Andrés, J. Bergmann, T. Dickel, J. Dilling, A. Ja-

cobs, A. Kwiatkowski, W. Plaß, C. Scheidenberger, D. Short, C. Will, C. Babcock, E. Dunling, A. Finlay, C. Hornung, C. Jesch, R. Klawitter, B. Kootte, D. Lascar, E. Leistenschneider, T. Murböck, S. Paul, M. Yavor, Commissioning and performance of TITAN's multiple-reflection time-of-flight mass-spectrometer and isobar separator, Nucl. Instrum. Methods A 1018 (2021) 165823. doi:10.1016/j.nima.2021.165823.

[12] F. Wienholtz, D. Beck, K. Blaum, C. Borgmann, M. Breitenfeldt, R. B. Cakirli, S. George, F. Herfurth, J. D. Holt, M. Kowalska, S. Kreim, D. Lunney, V. Manea, J. Menendez, D. Neidherr, M. Rosenbusch, L. Schweikhard, A. Schwenk, J. Simonis, J. Stanja, R. N. Wolf, K. Zuber, Masses of exotic calcium isotopes pin down nuclear forces, Nature 498 (7454) (2013) 346–349. doi:10.1038/nature12226.

[13] D. Atanasov, P. Ascher, K. Blaum, R. B. Cakirli, T. E. Cocolios, S. George, S. Goriely, F. Herfurth, H.-T. Janka, O. Just, M. Kowalska, S. Kreim, D. Kisler, Y. A. Litvinov, D. Lunney, V. Manea, D. Neidherr, M. Rosenbusch, L. Schweikhard, A. Welker, F. Wienholtz, R. N. Wolf, K. Zuber, Precision mass measurements of $^{129-131}$Cd and their impact on stellar nucleosynthesis via the rapid neutron capture process, Phys. Rev. Lett. 115 (2015) 232501. doi:10.1103/PhysRevLett.115.232501.

[14] M. Rosenbusch, P. Ascher, D. Atanasov, C. Barbieri, D. Beck, K. Blaum, C. Borgmann, M. Breitenfeldt, R. B. Cakirli, A. Cipollone, S. George, F. Herfurth, M. Kowalska, S. Kreim, D. Lunney, V. Manea, P. Navrátil, D. Neidherr, L. Schweikhard, V. Somà, J. Stanja, F. Wienholtz, R. N. Wolf, K. Zuber, Probing the $N = 32$ shell closure below the magic proton

number $Z = 20$: Mass measurements of the exotic isotopes ^{52,53}K, Phys. Rev. Lett. 114 (20) (2015) 202501. doi:10.1103/PhysRevLett.114.202501.

[15] E. Leistenschneider, M. P. Reiter, S. Ayet San Andrés, B. Kootte, J. D. Holt, P. Navrátil, C. Babcock, C. Barbieri, B. R. Barquest, J. Bergmann, J. Bollig, T. Brunner, E. Dunling, A. Finlay, H. Geissel, L. Graham, F. Greiner, H. Hergert, C. Hornung, C. Jesch, R. Klawitter, Y. Lan, D. Lascar, K. G. Leach, W. Lippert, J. E. McKay, S. F. Paul, A. Schwenk, D. Short, J. Simonis, V. Somà, R. Steinbrügge, S. R. Stroberg, R. Thompson, M. E. Wieser, C. Will, M. Yavor, C. Andreoiu, T. Dickel, I. Dillmann, G. Gwinner, W. R. Plaß, C. Scheidenberger, A. A. Kwiatkowski, J. Dilling, Dawning of the $N = 32$ shell closure seen through precision mass measurements of neutron-rich titanium isotopes, Phys. Rev. Lett. 120 (6) (2018) 062503. doi:10.1103/PhysRevLett.120.062503.

[16] Y. Ito, P. Schury, M. Wada, F. Arai, H. Haba, Y. Hirayama, S. Ishizawa, D. Kaji, S. Kimura, H. Koura, M. MacCormick, H. Miyatake, J. Y. Moon, K. Morimoto, K. Morita, M. Mukai, I. Murray, T. Niwase, K. Okada, A. Ozawa, M. Rosenbusch, A. Takamine, T. Tanaka, Y. X. Watanabe, H. Wollnik, S. Yamaki, First direct mass measurements of nuclides around $Z = 100$ with a multireflection time-of-flight mass spectrograph, Phys. Rev. Lett. 120 (15) (2018) 152501. doi:10.1103/PhysRevLett.120.152501.

[17] P. Schury, T. Niwase, M. Wada, P. Brionnet, S. Chen, T. Hashimoto,

H. Haba, Y. Hirayama, D. S. Hou, S. Iimura, H. Ishiyama, S. Ishizawa, Y. Ito, D. Kaji, S. Kimura, H. Koura, J. J. Liu, H. Miyatake, J.-Y. Moon, K. Morimoto, K. Morita, D. Nagae, M. Rosenbusch, A. Takamine, Y. X. Watanabe, H. Wollnik, W. Xian, S. X. Yan, First high-precision direct determination of the atomic mass of a superheavy nuclide, Phys. Rev. C 104 (2) (2021) L021304. doi:10.1103/PhysRevC.104.L021304.

[18] R. N. Wolf, D. Beck, K. Blaum, C. Böhm, C. Borgmann, M. Breitenfeldt, N. Chamel, S. Goriely, F. Herfurth, M. Kowalska, S. Kreim, D. Lunney, V. Manea, E. Minaya Ramirez, S. Naimi, D. Neidherr, M. Rosenbusch, L. Schweikhard, J. Stanja, F. Wienholtz, K. Zuber, Plumbing neutron stars to new depths with the binding energy of the exotic nuclide ^{82}Zn, Phys. Rev. Lett. 110 (2013) 041101. doi:10.1103/PhysRevLett.110.041101.

[19] A. Welker, N. A. S. Althubiti, D. Atanasov, K. Blaum, T. E. Cocolios, F. Herfurth, S. Kreim, D. Lunney, V. Manea, M. Mougeot, D. Neidherr, F. Nowacki, A. Poves, M. Rosenbusch, L. Schweikhard, F. Wienholtz, R. N. Wolf, K. Zuber, Binding energy of ^{79}Cu: Probing the structure of the doubly magic ^{78}Ni from only one proton away, Phys. Rev. Lett. 119 (19) (2017) 192502. doi:10.1103/PhysRevLett.119.192502.

[20] W. R. Plaß, T. Dickel, C. Scheidenberger, Multiple-reflection time-of-flight mass spectrometry, Int. J. Mass. Spectrom. 349-350 (2013) 134–144. doi:10.1016/j.ijms.2013.06.005.

[21] Z. Y. Zhang, L. Ma, Z. G. Gan, M. H. Huang, T. H. Huang, G. S. Li, X. L. Wu, G. B. Jia, L. Yu, H. B. Yang, Z. Y. Sun, X. H. Zhou, H. S.

Xu, W. L. Zhan, A gas-filled recoil separator, SHANS, Nucl. Instrum. Methods B 317 (2013) 315–318. doi:10.1016/j.nimb.2013.05.062.

[22] J.-Y. Wang, Y.-L. Tian, Y.-S. Wang, Z.-G. Gan, X.-H. Zhou, H.-S. Xu, W.-X. Huang, A multi-reflection time-of-flight mass analyzer at IMP/CAS, Nucl. Instr. Methods B 463 (2020) 179–183. doi:10.1016/j.nimb.2019.05.067.

[23] W. R. Plaß, T. Dickel, U. Czok, H. Geissel, M. Petrick, K. Reinheimer, C. Scheidenberger, M. I.Yavor, Isobar separation by time-of-flight mass spectrometry for low-energy radioactive ion beam facilities, Nucl. Instrum. Methods B 266 (19) (2008) 4560–4564. doi:10.1016/j.nimb.2008.05.079.

[24] H. B. Pedersen, D. Strasser, S. Ring, O. Heber, M. L. Rappaport, Y. Rudich, I. Sagi, D. Zajfman, Ion motion synchronization in an ion-trap resonator, Phys. Rev. Lett. 87 (5) (2001) 055001. doi:10.1103/PhysRevLett.87.055001.

[25] R. N. Wolf, F. Wienholtz, D. Atanasov, D. Beck, K. Blaum, C. Borgmann, F. Herfurth, M. Kowalska, S. Kreim, Y. A. Litvinov, D. Lunney, V. Manea, D. Neidherr, M. Rosenbusch, L. Schweikhard, J. Stanja, K. Zuber, ISOLTRAP's multi-reflection time-of-flight mass separator/spectrometer, Int. J. Mass Spectrom. 349-350 (2013) 123–133. doi:10.1016/j.ijms.2013.03.020.

[26] W.-X. Huang, Y.-L. Tian, Y.-S. Wang, J.-Y. Wang, X.-H. Zhou, Optimization of multi-reflection time-of-flight mass analyzer operating

in in-trap-lift mode, Radiat Detect Technol Methods 2 (1) (2018) 1. doi:10.1007/s41605-017-0031-1.

[27] https://www.cathode.com/i_alkali.htm.

[28] N. E. Bradbury, R. A. Nielsen, Absolute values of the electron mobility in hydrogen, Phys. Rev. 49 (1936) 388–393. doi:10.1103/PhysRev.49.388.

[29] R. N. Wolf, G. Marx, M. Rosenbusch, L. Schweikhard, Static-mirror ion capture and time focusing for electrostatic ion-beam traps and multi-reflection time-of-flight mass analyzers by use of an in-trap potential lift, Int. J. Mass Spectrom. 313 (2012) 8–14. doi:10.1016/j.ijms.2011.12.006.

[30] https://www.etp-ms.com.

[31] https://thinksrs.com/index.html.

[32] https://www.edwardsvacuum.com/en.

[33] https://iseg-hv.com/en/home.

[34] https://www.behlke.com/.

[35] http://www.cgc-instruments.com/.

[36] https://epics.anl.gov.

[37] http://www.ni.com/.

[38] S. Purushothaman, S. Ayet San Andrés, J. Bergmann, T. Dickel, J. Ebert, H. Geissel, C. Hornung, W. R. Plaß, C. Rappold, C. Scheidenberger, Y. K. Tanaka, M. I. Yavor, Hyper-EMG: A new probability distribution function composed of exponentially modified gaussian distributions to analyze asymmetric peak shapes in high-resolution time-of-flight mass spectrometry, Int. J. Mass Spectrom. 421 (2017) 245–254. doi:10.1016/j.ijms.2017.07.014.

[39] D. J. Manura, D. A. Dahl, SIMION 8.0/8.1 User Manual, Scientific Instrument Services, Inc., Idaho National Laboratory, 2011.